Origins of radiation-induced attenuation in pure-silica-core and Ge-doped optical fibers under pulsed x-ray irradiation

V. De Michele [iD], C. Marcandella, J. Vidalot, P. Paillet, A. Morana [iD], M. Cannas [iD], A. Boukenter [iD], E. Marin [iD], Y. Ouerdane [iD], and S. Girard [iD]

View Online   Export Citation   CrossMark

Origins of radiation-induced attenuation in pure-silica-core and Ge-doped optical fibers under pulsed x-ray irradiation

V. De Michele,[1,2,a)] C. Marcandella,[3] J. Vidalot,[1,3] P. Paillet,[3] A. Morana,[1] M. Cannas,[2] A. Boukenter,[1] E. Marin,[1] Y. Ouerdane,[1] and S. Girard[1]

AFFILIATIONS

[1]Univ Lyon, UJM, CNRS, IOGS, Laboratoire H. Curien, UMR 5516, 42000 Saint Etienne, France
[2]Department of Physics and Chemistry "Emilio Segrè," University of Palermo, Via Archirafi 36, 90123 Palermo, Italy
[3]CEA, DAM, DIF, F-91297 Arpajon, France

a)Author to whom correspondence should be addressed: vincenzo.demichele@univ-st-etienne.fr

ABSTRACT

We investigated the nature, optical properties, and decay kinetics of point defects causing large transient attenuation increase observed in silica-based optical fibers exposed to short duration and high-dose rate x-ray pulses. The transient radiation-induced attenuation (RIA) spectra of pure-silica-core (PSC), Ge-doped, F-doped, and Ge + F-doped optical fibers (OFs) were acquired after the ionizing pulse in the spectral range of [∼0.8–∼3.2] eV (∼1500–∼380 nm), from a few ms to several minutes after the pulse, at both room temperature (RT) and liquid nitrogen temperature (LNT). Comparing the fiber behavior at both temperatures better highlights the thermally unstable point defects contribution to the RIA. The transient RIA origin and decay kinetics are discussed on the basis of already-known defects absorbing in the investigated spectral range. These measurements reveal the importance of intrinsic metastable defects such as self-trapped holes (STHs), not only for PSC and F-doped fibers but also for germanosilicate optical fibers as clearly evidenced by our LNT measurements. Furthermore, our results show that fluorine co-doping seems to decrease the RIA related to the strain-assisted STHs absorption bands in both types of optical fibers. Regarding Ge-doped glasses, besides a description of the defects responsible of the RIA, highlighting the STHs' role in their transient response, we provide a clear correlation between the GeX and GeY centers' kinetics. In conclusion, the presented results improve our understanding of the transient RIA origin in the ultraviolet and visible domains. The lack of knowledge about the defects causing the RIA in the near-infrared domain will require future studies.

I. INTRODUCTION

The continuous development of new optical fiber (OF) classes has motivated the research community to apply them to different and innovative technological domains such as telecommunications, innovative sensors for structural health monitoring, diagnostics, and even radiation dosimetry.[1–3] Furthermore, in recent years, OFs are more commonly used in systems or sub-systems having to operate in severe radiation-rich environments, e.g., in space missions.[4,5] This interest is explained by the fact that optical fibers globally present a good tolerance to ionizing and non-ionizing radiations compared to microelectronic technologies and are also immune to most electromagnetic perturbations. As a consequence, optical fibers are used for a variety of needs in fusion-devoted facilities such as the Laser Mégajoule in France and the National Ignition Facility in the USA.[6–10] For these infrastructures, the plasma and laser fiber-based diagnostics have then to survive a series of ignition shots that will be associated with a burst of x-rays, γ-rays, and 14 MeV neutrons.[11] Under transient radiation exposure, the waveguide transmission capability is strongly reduced by the radiation-induced attenuation (RIA) phenomenon as well as by parasitic light generation through radiation-induced emission (RIE). The origin of these deleterious effects comes from point defect generation in the silica-based fiber core and cladding absorbing light through inter-band electronic levels.[4,12–14] Accordingly, studying the basic mechanisms governing the generation and the

recovery of those point defects remains crucial to better understand the fiber response. Basically, we can estimate its vulnerability for its given profile of use and, when needed, to propose ways to improve its radiation tolerance to fulfill the application requirements. In order to enhance our understanding of the basic mechanisms explaining the fiber radiation response, it is crucial to have a complete knowledge of all the fiber intrinsic parameters known to influence its radiation response, such as its core and cladding composition, the potential treatments applied on either the preform or the fiber.[4,5] This is why, instead of using commercial samples for such studies, it is preferable to use the so-called "canonical samples"[12,13,15] that are manufactured specifically for these studies, knowing all their details, while having similar radiation responses to the same type of commercial ones. Moreover, controlling the manufacturing parameters enables us to adapt the refractive index profile through fiber doping and highlight the influence of a co-dopant, such as fluorine in this study. The PSC and Ge-doped fibers represent the most radiation tolerant fibers[14] for the environments associated with steady state ionizing irradiation (such as those encountered in space and nuclear industry) while those containing Al or P present RIA levels largely higher and can only be used for radiation detection or dosimetry applications.[14,15] It is interesting to note that under transient irradiation (pulsed irradiation), such as the one associated with ignition experiments at LMJ or NIF, the PSC and Ge-doped fibers still present the best performances at longer times after the shots, as depicted in Fig. 1 of Ref. 16. However, at earlier times, where most of the diagnostics have to operate, the RIA levels could be higher than in the P-doped optical fiber due to the generation of room temperature metastable defects with strong absorption levels.[14–17] To overcome the complexity to study the fibers' response at the shortest times, it is possible to lower the irradiation temperature (LNT in our experimental conditions), thereby slowing down the decay kinetics of these metastable defects. Decreasing the irradiation temperature allows studying the RT metastable defect contribution (impacting at time <1 ms at RT) even with a temporal resolution around hundreds of milliseconds. The PSC OFs have been investigated in similar experimental conditions,[16,18–21] highlighting the strong contribution of the STHs' related absorption bands[14,20–24] and of chlorine impurities.[25,26] The Ge-doped OFs still deserve such investigation since they are the most used waveguides for telecommunications or sensing with fiber Bragg gratings thanks to their ultraviolet photosensitivity, related to the physics of GeX, Ge(1), and GLPC[14] defects. It is known that the germanosilicate OFs radiation response at RT is more driven by Ge-related defects[27–30] than by Si-defects and that most of them are associated with absorption bands peaking in the UV[14] spectral domain. An increase in attenuation under steady state ionizing radiation was observed at LNT, suggesting the presence of transient defects such as STHs.[15,31] The hypothesis of the STHs' presence in the Ge-doped OFs justifies their transient response investigation, especially if compared to PSC OFs for which the STH key role on the fiber darkening at LNT is now widely accepted. Furthermore, the present study also investigates the fluorine doping influence on its radiation response. It is well known from previous studies that fluorine could reduce the number of precursor sites such as the strained Si–O–Si bonds that are converted into strain-assisted (s-a) STH defects under radiation

exposure.[32,34] The purpose of the present work is to study the RIA kinetics after the x-ray pulse, evaluating the PSC, F-doped, Ge-doped, and Ge + F-codoped OFs. The investigation was performed analyzing the observed differences in terms of RIA levels and kinetics at RT and LNT in the spectral range between ~0.8 eV and ~3.2 eV (~1500–~380 nm) and in a time window of hundreds of seconds. Moreover, the RIA spectra were decomposed using a set of Gaussian bands related to already known defects to identify the center structure causing this excess loss.

II. EXPERIMENTAL SETUP

The pulsed ~1 MeV x-ray radiation responses of our fibers were characterized using the ASTERIX facility from CEA[35] (pulse duration around tens of nanoseconds) simulating the dose rates associated with the ignition shots at megajoule class laser facilities.[36,37] These experimental conditions lead to very high dose rates (>1 MGy/s) and moderate accumulated doses [on the order of ~10 Gy(SiO_2)]. The dose and dose rate are adjusted by varying the distance between the x-ray source and the fiber under test.

The online RIA measurements allow us to characterize the transient fiber response as a function of time, from a few milliseconds to a few minutes after the x-ray shot. We characterized several canonical optical fibers from iXblue manufacturer,[38] with varying core compositions: PSC, F-, Ge-, and Ge + F-doped fibers. In Figs. 1(a) and 1(b), the fluorine and germanium radial distributions in the F- and Ge-doped samples, respectively, as measured by energy dispersive x-ray analysis (EDX) are reported.

The F content in the fluorine doped sample cores is ~0.25 wt. % and ~0.1 wt. % for the F-doped and Ge + F-codoped OFs, respectively. The germanium content in both Ge-doped fiber cores under test (FUT) is around 8.5 wt. %. For the Ge + F canonical sample, the F content and distribution were chosen to present the same refractive index profile than the Ge-doped OF. For all the samples, the SiOH groups' concentration is below 10 ppb. This threshold, given by the manufacturer, is deduced from the fact that no 1380 nm absorption peak could be detected in the manufactured samples. The chlorine impurities concentration has been measured by energy-dispersive x-ray (EDX) spectroscopy and is around 0.2 wt. % in the whole set of samples, while the other impurities are below the 100 ppm, limit of the EDX analysis. Fiber characteristics are summarized in Table I.

The experimental setup is depicted in Fig. 2: the fiber is coiled within a 80 mm diameter and its length is adjusted with respect to expected radiation sensitivity. As shown in Fig. 2, the FUT are connected with FC-PC connectors to rad hard fiber pigtails allowing the transport of the signal between the instrumentation and the irradiation zones. FUT's input ends are connected to a white light Deuterium–Halogen source (Ocean Optics DH-200-BAL) and their outputs to miniature spectrometers (Maya 2000 spectrometers for the UV-Vis measurements and the NIR512 spectrometer for IR measurements, both from Ocean Optics), within tenths of milliseconds resolution time.

For LNT measurements, the fibers were located in a container filled with liquid nitrogen: the experiments started after full fiber thermalization. In order to guarantee the same dose and dose rate for the measurements in both UV/visible and near-IR ranges, these data acquisitions were performed simultaneously (during the same shot).
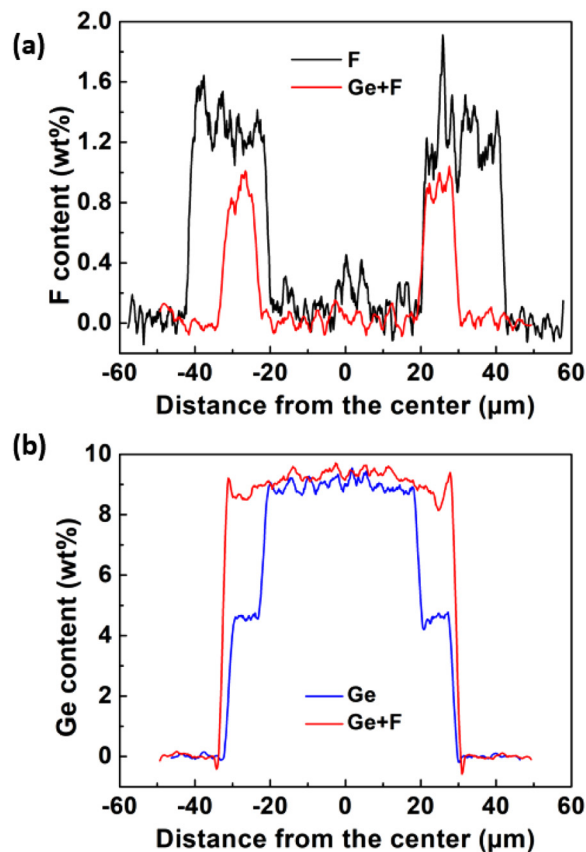
FIG. 1. (a) Fluorine and (b) germanium radial distributions in the F-doped and Ge-doped samples, respectively, measured by EDX analysis.

III. EXPERIMENTAL RESULTS

Figures 3(a) and 3(b) report the RIA spectra acquired 1 s after the x-ray pulse, between 380 nm and 1500 nm for the four fibers, at RT and LNT, respectively. At RT [Fig. 3(a)], the fibers' RIA spectra seem to be explained by the tail(s) of UV absorption band(s). For the PSC OF, the involved defects are probably those associated with chlorine impurities and a small contribution from both SiE′ and NBOH[39,40] centers, having absorption bands centered at ∼215 nm and ∼260 nm. It is important to underline that the main contributor in the UV part of the investigated spectral range is due to the Cl-related defects, as already observed in Refs. 33 and 41 for other irradiation conditions on the same samples, where above 3 eV, it was observed that the SiE′ and NBOHC contributions to the RIA remain negligible. While for Ge-doped fibers, we can have the contributions of GeX and Ge(1) centers with absorption signatures around 475 nm and 280 nm, respectively. Despite the different origins for RIA, the various fiber induced loss levels are comparable. The F co-doping impact differs for the PSC and Ge-doped fibers: the RIA of the F-doped and the PSC OFs show only a slight difference, whereas the Ge + F-doped OF is more radiation tolerant than the Ge-doped one.

At LNT [Fig. 3(b)], the RIA levels and spectra are different compared to RT results. The RIA spectra are more defined as losses are higher, highlighting new spectral features more clearly, probably composed of more bands, around 500–600 nm. These new profiles can be explained by the major contribution of new absorption bands, as already observed under pulsed and steady state x- and γ-rays.[15,20,21,42] At least for the PSC, these bands were interpreted as the manifestation of STHs at low temperature. STHs are associated with several absorption bands peaking between 1.6–1.88 eV and 2.16–2.6 eV. The absence of these defects in the spectra at RT can be explained by their strong instability in these conditions and the disappearance of their contribution within a millisecond time scale.

At LNT, the RIA observed for the Ge- and Ge + F-doped OFs is at least one order of magnitude higher compared to RT measurements. The RIA increase is observed even for the PSC and F-doped OFs: RIA at LNT is about three times higher than at RT. All these observations are confirmed even for longer times, as highlighted by the 650 nm RIA decay kinetics shown in Figs. 4(a) and 4(b) at RT and LNT, respectively. The ability of LNT to slowdown the defect decay kinetics is obvious: the PSC RIA is reduced by a factor of 10 at RT in the 100 ms–100 s time window, while at LNT, RIA is only reduced by a factor of 2 over the same period.

TABLE I. Samples, dopant nature and amounts in the core, used sample lengths for irradiation tests, Δn, core, cladding and coating dimension, and the initial loss measured at 1310 nm.

Fiber	PSC	F-doped	Ge-doped	Ge + F-doped
F content in the core (wt. %)	None	0.25	None	0.1
Ge content in the core (wt. %)	None	None	8.5	8.5
UV/visible RT length (m)	10	10	1	10
Near-IR RT length (m)	50	50	10	50
UV/visible LNT length (m)	1	10	1	1
Near-IR LNT length (m)	1	50	10	50
Δn ($\times 10^{-3}$)	5.3	5	9	9
Core dimension (μm)	62.5	42.5	62.5	62.5
Cladding dimension (μm)	125	125	125	125
Coating dimension (μm)	250	250	250	250
Initial loss @ 1310 nm (dB/km)	10	6	2	2
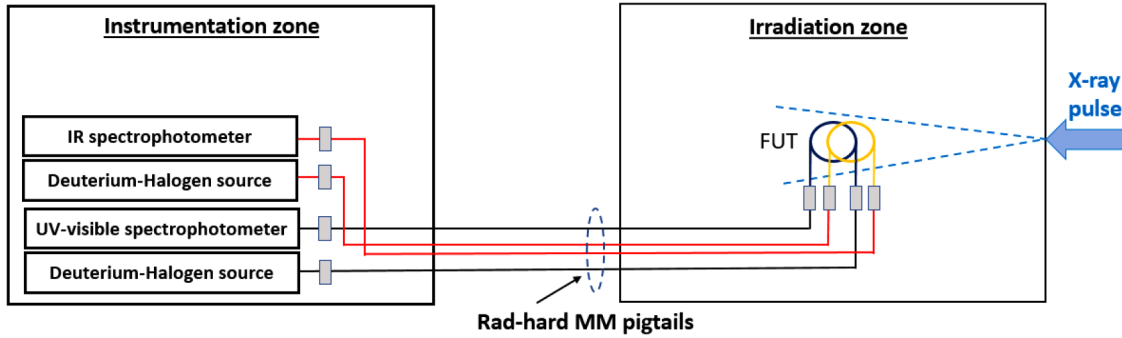
FIG. 2. Experimental setup for online RIA measurements at ASTERIX pulsed x-ray facility.

IV. DISCUSSION

A. PSC and F-doped OFs

To highlight the difference between the RIA spectra acquired at both temperatures and to better determine the fluorine doping influence on the induced losses, we reproduced the RIA spectra using decomposition based on a set of Gaussian functions representing the point defects' absorption bands already discussed in the literature. A Gaussian band is defined by

$$G(x) = A \frac{2\sqrt{\ln(2)}}{\sqrt{\pi}\ \text{FWHM}} e^{-\left[\frac{2\sqrt{\ln(2)}}{\text{FWHM}}(x-x_c)\right]^2},$$

where A is the band area, x_c is the center of the optical absorption (OA) band, and FWHM is the full width at half maximum.
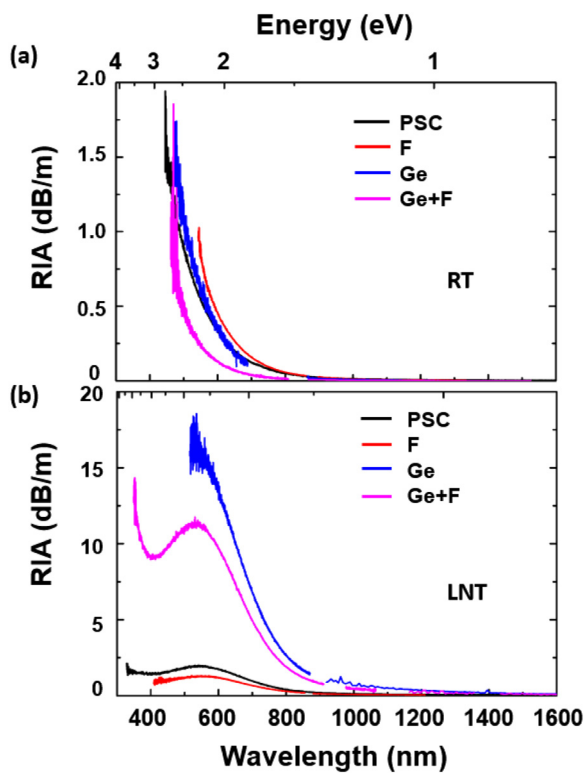
FIG. 3. RIA spectra recorded 1 s after the x-ray pulse at RT (a) and at LNT (b) at ∼10 Gy(SiO₂) of the accumulated dose: PSC OF in black line, F-doped OF in red, Ge-doped OF in blue, and Ge + F-doped OF in magenta.
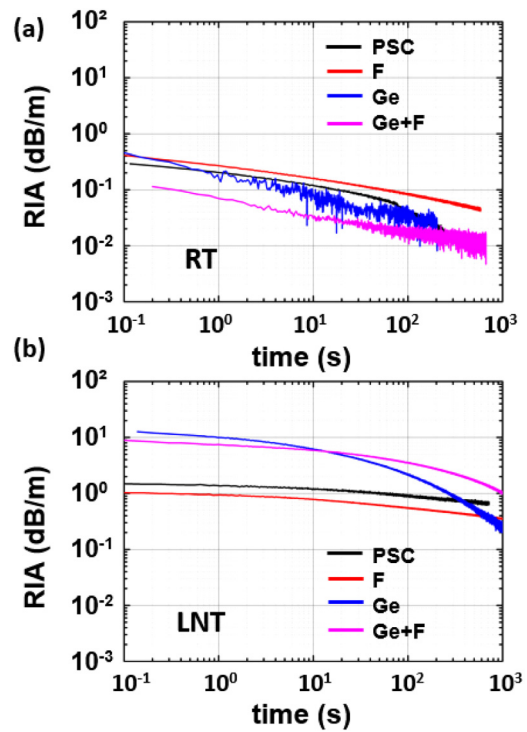
FIG. 4. Post-pulse recovery kinetics for the four different optical fibers at 650 nm at ∼10 Gy(SiO₂) of the accumulated dose at RT (a) and LNT (b): PSC in black, F-doped in red, Ge-doped in blue, and Ge + F-doped in magenta.

TABLE II. Parameters of the Gaussian absorption bands associated with a variety of pure silica related defects. This set, from Ref. 14, serves to reproduce the acquired RIA spectra.

Defect	OA peak (eV)	FWHM (eV)	PSC RT (dB/m)	PSC LNT (dB/m)	F-doped RT (dB/m)	F-doped LNT (dB/m)
S-a STH$_2$	1.63	0.6		0.10		0.07
S-a STH$_1$	1.88	0.5		0.13		0.10
STH$_2$	2.16	0.6		0.50		0.30
STH$_1$	2.61	1.2	0.50	1.60	0.50	1.30
Cl^0	3.26	1.2	2.40	0.70	5.00	0.04
Cl$_2$	3.78	0.7	2.90	0.90	6.00	2.10

The fitting routine consists in using a set of Gaussian bands with fixed parameters, such as the center of the Gaussian and its FWHM, taken from Ref. 14. The Gaussian area is the free parameter and is proportional to the defect's concentration and oscillator strength. The obtained results are reported in Table II and Fig. 5 for both the PSC and the F-doped fibers. Point defects for which the optical absorption band area is under the detection limit of our analysis are not reported. They may exist in the irradiated optical fibers but do not contribute significantly to the measured RIA.

At RT, as illustrated in Figs. 5(a) and 5(c), the spectrum in the UV/visible range is quite well reproduced with a limited set of specific defects associated with chlorine impurities (Cl^0 and Cl$_2$ and their absorption bands at 3.26 eV and 3.78 eV, respectively) and the inherent STH$_1$ (absorption band at 2.6 eV). The same decomposition is valid for both fibers: a higher relative contribution of

Cl-related defects is observed in the F-doped fiber, justifying the slightly higher RIA level in the UV for this fiber [see Fig. 3(a)]. Nevertheless, a lack of knowledge regarding the RIA contribution in the NIR is obvious, resulting in an underestimation of the RIA in this spectral range by the theoretical curve using the available set of defects.

As mentioned above and shown in Figs. 5(b) and 5(d) for the LNT measurements, the new spectral features between ~1.5 eV and ~2 eV are attributed to the STHs' related absorption bands, such as the strain-assisted STH$_2$ peaked at 1.63 eV, the strain-assisted STH$_1$ peaked at 1.88 eV, and the inherent STH$_2$ peaked at 2.16 eV.

These absorption bands are strongly unstable at RT and are typically observed at low temperature in these experimental conditions.[15] Moreover, the inherent STH$_1$ amount increased by a factor of ~3 for both samples. These results, consistent with those observed in Ref. 15, show a decrease in the Cl^0 band contribution for both fibers at LNT, thereby supporting the hypothesis from Griscom *et al.* of the inter-dependence between STHs and Cl^0 defects.[43] Even at LNT, it is not possible to reproduce the RIA profile in the NIR, as depicted in Figs. 5(b) and 5(d), as for the RT measurements: below ~1.5 eV, the fitting curve does not match the experimental data. The missing contribution, especially at LNT, could be one of the non-Gaussian absorption bands, the so-called low-temperature-infrared-absorption (LTIRA), attributed to strain-assisted STHs.[20,24] In fact, the difference between the theoretical function and the experimental data is higher at LNT, where the appearance of the strain-assisted STHs' bands is more probable. A recent work[44] attributes this discrepancy to new absorption bands linked to the STH and peaking around 1 eV (not used in our decomposition). Therefore, the above-mentioned fitting routine allows the experimental data reproduction, up to

FIG. 5. Decomposition of the RIA spectra measured 1 s after the x-ray pulse, at ~10 Gy(SiO$_2$) of the accumulated dose, for the PSC [(a) RT and (b) LNT] and for the F-doped [(c) RT and (d) LNT] fibers: open circles are the experimental data, red lines are the global fitting functions, the brown and gray lines are the strain-assisted STH$_2$ and strain-assisted STH$_1$ contributions, green and blue are the inherent STH$_2$ and inherent STH$_1$, and orange and purple are the Cl^0 and the Cl$_2$ defect contributions.
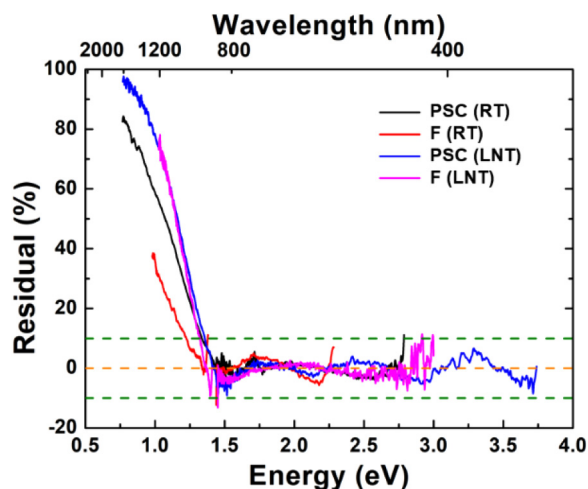
FIG. 6. Normalized residuals between the experimental RIA data and the global fitting function: in black for the PSC OF at RT, in red for the F-doped OF at RT, in blue for the PSC OF at LNT, and in magenta for the F-doped OF at LNT. The green and the orange dashed lines are guide lines for ±10% and 0%, respectively.

1.5 eV, at both temperatures within a 10% error, as highlighted in Fig. 6, where the normalized residuals between the experimental data and the global fitting function are reported. The discrepancy in the NIR spectral range lies between 40% and 80% at RT and even 100% at LNT for the longer wavelengths. In this spectral domain, data could not be fitted by only one Gaussian curve, supporting the hypothesis made in Ref. 44. Clearly, further studies are still needed to clarify this contribution.

B. Ge- and Ge + F-doped OFs

The same fitting procedure was employed to better analyze the Ge- and Ge + F-doped optical fibers, as depicted in Fig. 7. In this case, the set of defects comprising both Si- and Ge-related defects, from Ref. 14, was used, and their main characteristics are given in the Table III. At RT [Figs. 7(a) and 7(c)], the experimental data are quite well reproduced using the GeY OA band at 1.38 eV[30] and by the defect tails with absorption bands in the UV: GeX at 2.6 eV, the so-called "transient defect" (TD) at 3.26 eV, already observed after x-ray pulses,[14,45] and of Ge(1) defect absorbing at 4.4 eV. By comparing the Ge and Ge + F fibers, it is observed, contrary to the Ge(1) contribution, that it increases by a factor of 2 (even if this band with the peak far away from the experimental data has a higher uncertainty in the fitting routine), a general decrease in the defect contributions for the Ge + F fiber, justifying its higher radiation tolerance noted at RT in Fig. 3.

Even at LNT [Figs. 7(b) and 7(d)], the discrepancy between the experimental data and the fit remains within the experimental data dispersion, meaning that the set of defects is able to reproduce the RIA spectra. As already observed previously,[15,20] at low temperature, the RIA of the Ge-doped OF increases showing a strong temperature dependence of defect stabilities. Furthermore, the large differences in the RIA spectra are explained by the appearance of
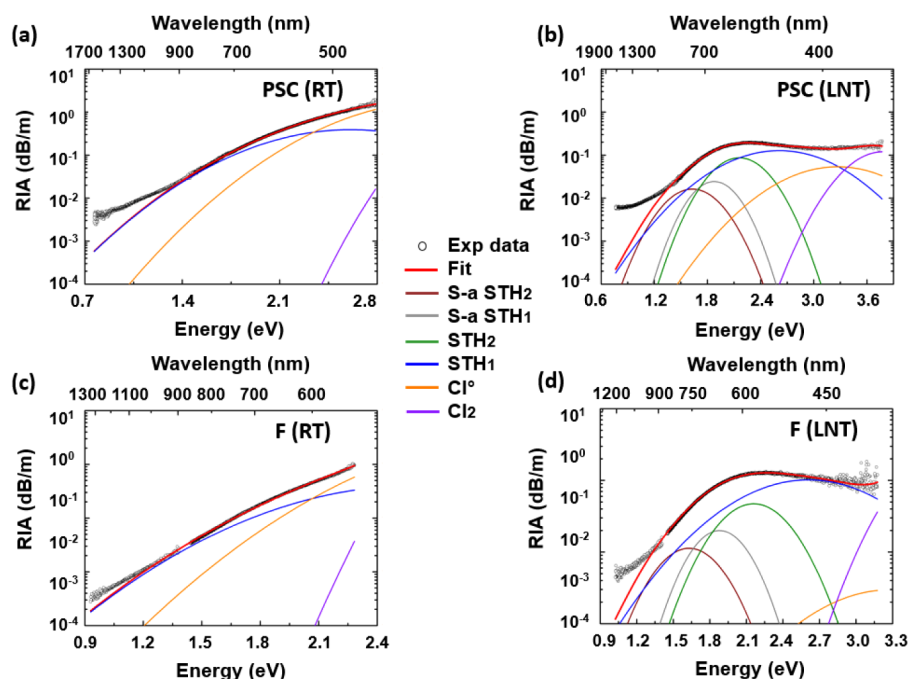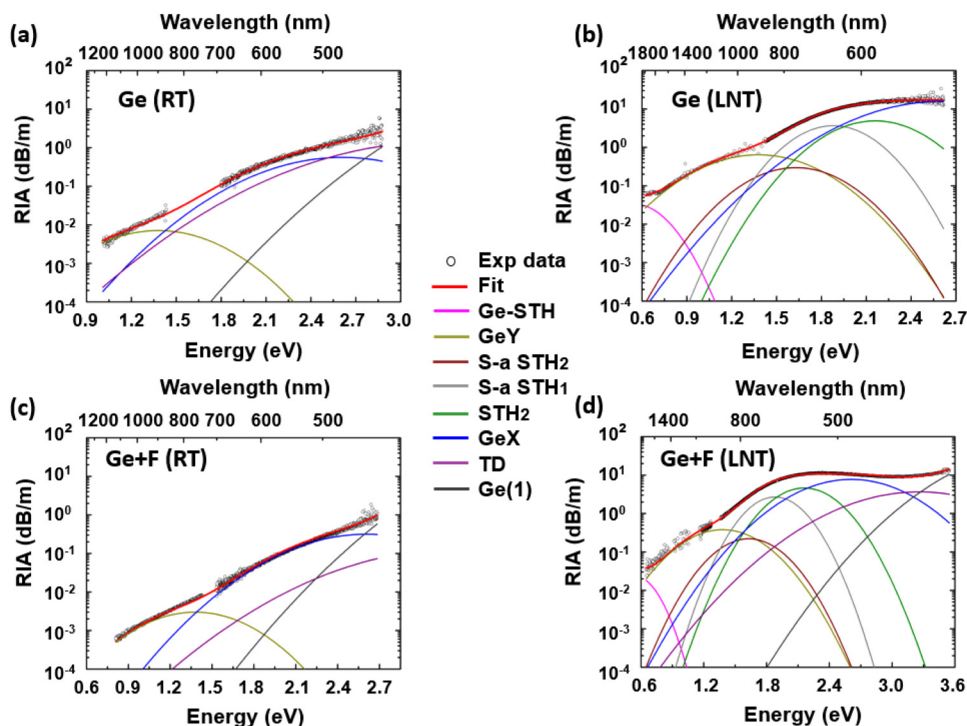

FIG. 7. Decomposition of the RIA spectra measured 1 s after the x-ray pulse, at ~10 Gy(SiO₂) of the accumulated dose, for the Ge-doped OF [(a) RT and (b) LNT] and for the Ge + F-doped OF [(c) RT and (d) LNT]: open circles are the experimental data, the red line is the global fitting function, pink is the Ge-STH contribution, yellow is the GeY band, brown and gray are the strain-assisted STH₂ and strain-assisted STH₁ contributions, respectively, green is the inherent STH₂ absorption band, blue is the GeX contribution, magenta is the transient defect, and dark gray is the Ge(1) absorption band.

TABLE III. Parameters of the Gaussian absorption bands associated with a variety of Ge- and Si-related defects. This set, from Ref. 14, was used to reproduce the acquired RIA spectra.

Defect	OA peak (eV)	FWHM (eV)	Ge RT (dB/m)	Ge LNT (dB/m)	Ge + F RT (dB/m)	Ge + F LNT (dB/m)
Ge-STH	0.54	0.35		0.014		0.01
GeY	1.38	0.71	0.006	0.48	0.002	0.3
S-a STH$_2$	1.63	0.60		0.20		0.14
S-a STH$_1$	1.88	0.50		1.90		1.4
STH$_2$	2.16	0.60		3.00		3.0
GeX	2.60	0.97	0.60	16	0.15	8.0
TD	3.26	1.30	1.9		0.81	5.0
Ge(1)	4.40	1.20	180		200	54

FIG. 8. Normalized residuals between the RIA experimental data and the global fitting function: black for the Ge-doped OF at RT, red for the Ge + F-doped OF, blue for the Ge-doped OF at LNT, and magenta for the Ge + F-doped OF at LNT. The green and the orange dashed lines are guide lines for ±10% and 0%, respectively.

new absorptions bands, especially around ∼1.5 eV and ∼2.0 eV, that are not related to known Ge-defects. As hypothesized in Ref. 15, the strain-assisted STHs appear to be good candidates to fill this discrepancy, having absorption bands in this spectral domain.

Indeed, these absorption bands were employed in our fitting routine, leading the theoretical function to quite well reproduce the experimental data. However, as expected, the transient defects present a much lower relative contribution to the total RIA at LNT, while the Ge(1) contribution decreases by a factor of 4; both defects start to be below our sensitivity threshold for the Ge-doped fiber while remaining discernable in the Ge + F-doped fiber response. The involved STHs' absorption bands are the Ge-STH ones that peaked at 0.54 eV, whereas those of strain-assisted STH$_2$ and strain-assisted STH$_1$ peaked, respectively, at 1.63 eV and 1.88 eV and the inherent STH$_2$ at 2.16 eV. The strain-assisted defects present a slightly lower area in the Ge + F-doped fibers, this may be explained by a precursor site concentration decrease due to F-doping.[33,34] The inherent STH$_1$ absorption band is not needed to reproduce our experimental data. This could be explained by the OA band overlap with the GeX one, in any case both defects should present similar temperature dependence. At the present analysis stage, it is difficult to discuss the exact temperature dependence of Ge-related defects. For example, our results regarding GeX differ from those of Ref. 30, where the authors observed an opposite trend, with an increase in GeX concentration with the temperature. However, it should be reminded that the irradiation temperature effect on a single defect behavior is strongly dependent on irradiation conditions (dose, dose rate, and temperature) and could then have either a negative or positive impact on the RIA depending on the exact test conditions [this is more discussed in Ref. 46 for the Ge(1) case]. More systematic experiments are then needed to clarify the defect dependencies as a function of irradiation temperature.

The quality of the fit is acceptable in the whole spectra, highlighting that the presence of germanium in the core prevents the unknown Si-related defect formation involved in the PSC and F-doped fiber responses. This is obvious from the normalized residuals between the experimental data and the global fitting
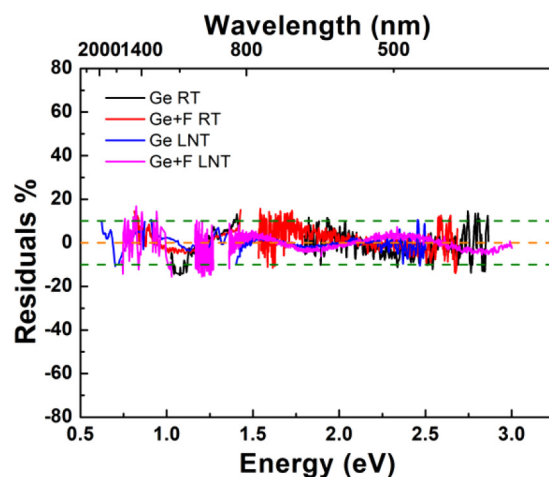
function, as reported in Fig. 8, in which the fit procedure quality is within ±10% for the whole spectral range.

C. Point defect kinetics

Applying the same fitting routine to all the recorded spectra up to 200 s after pulse (from 2000 to 20 000 spectra depending on the integration time on the order of tens of ms), it becomes possible to study the kinetics of each defect instead of the one of the total RIA at a given wavelength. For times longer than 200–300 s, the RIA value is closer to our detection limit, making the fitting routine less robust, and then these longer times were not been considered in our analysis. For the first 200 s after the shot, it was possible to achieve decomposition for the same spectral range (depending on each fiber type) keeping the same fitting quality than the one illustrated for the spectra acquired at 1 s after the pulse. After this analysis, we are then able to plot the intensity time evolution of each optical absorption band, highlighting the behaviors of different point defects. The obtained kinetics are illustrated in Figs. 9 and 10. Indeed, we reported the normalized decay kinetics of various point defects identified in PSC and F-doped OFs at RT and LNT in Fig. 9. Furthermore, the different kinetics are studied with the fractal formalism proposed by Griscom *et al.* in Ref. 47 by the following equation:

$$N[(kt)^\beta] = N(0)e^{-(kt)^\beta},$$

where $N[(kt)^\beta]$ is the defect concentration at a given time t, k is the decay-rate parameter, and β is linked to diffusion-controlled reactions and its value ranges between 0 and 1. The best fit curves are depicted in Fig. 9 for the defects involved in the fitting procedure.
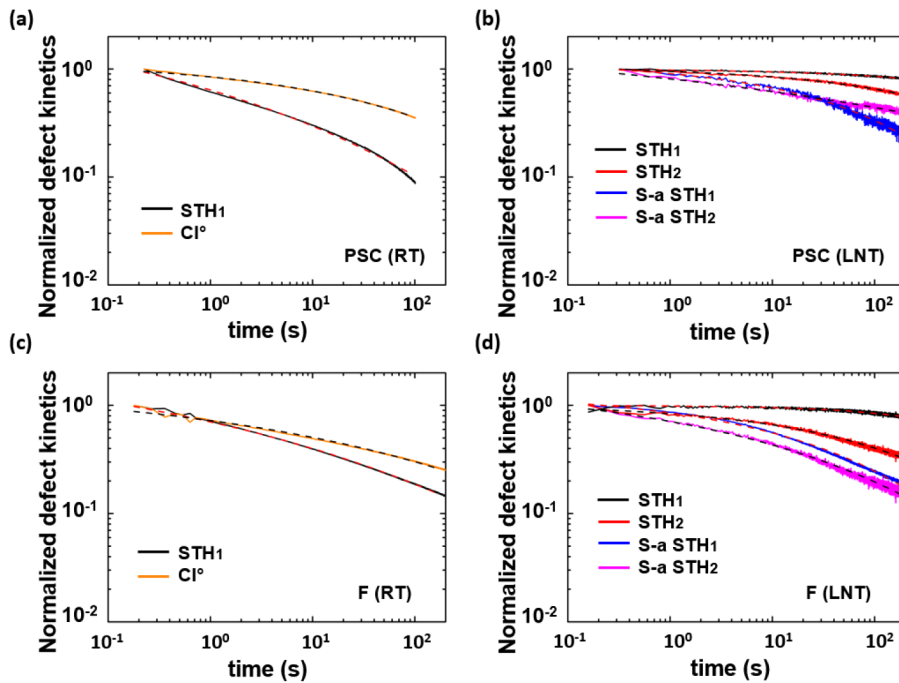
FIG. 9. Normalized decay kinetics of the defects as extracted from the fitting routine, at ∼10 Gy(SiO$_2$) of the accumulated dose, for the PSC and F-doped fibers, at RT (a) and (c) and at LNT (b) and (d). The lines in color are as follows: black is the STH$_1$, red is the STH$_2$, blue is the strain-assisted STH$_1$, magenta is the strain-assisted STH$_2$ and in orange the Cl^0. The dashed lines are the fits relative to the overlapped defects kinetics.

For a few defects listed in Table II, those decay kinetic parameters are too noisy in our test conditions to be analyzed in this paper.

There is a good quality fit for all the extracted defect kinetics at both temperatures, highlighting how the fractal model could well describe the experimental results. Comparing RT and LNT data, it is obvious that the additional STH-related absorption band contributions (STH$_2$, strain assisted STH$_1$, and STH$_2$) explain the different RIA spectra shapes at both temperatures. The different
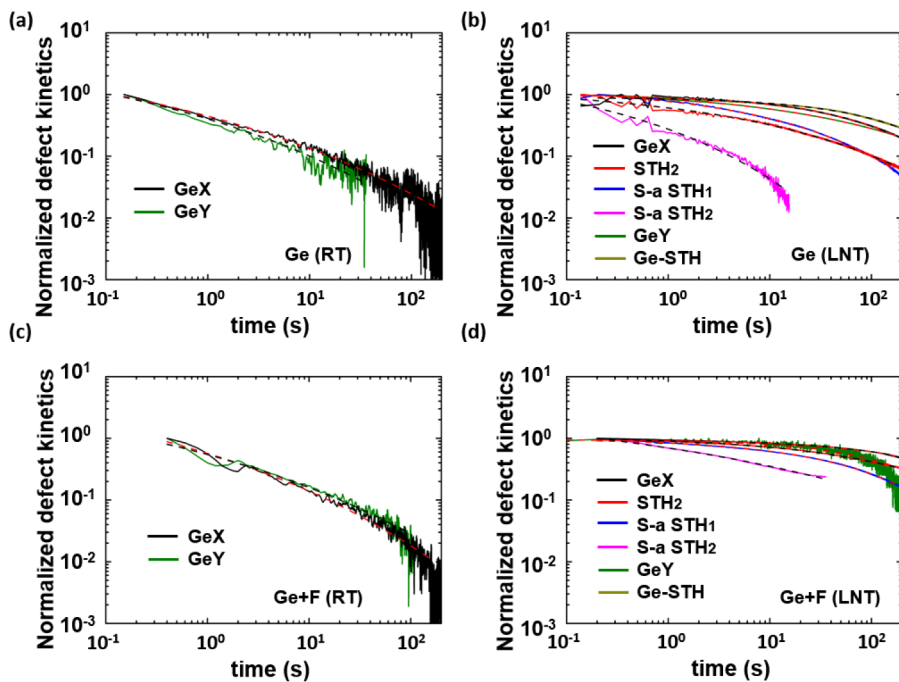
FIG. 10. Normalized decay kinetics of the defects as extracted from the fitting routine, at ∼10 Gy(SiO$_2$) of the accumulated dose, for the Ge- and Ge + F-doped samples, at RT (a) and (b) and at LNT (c) and (d). The lines in color are follows: black is the GeX, red is the STH2, blue is the strain-assisted STH$_1$, magenta is the strain-assisted STH$_2$; green is the GeY, and dark yellow is the Ge-STH. The dashed lines are the fits relative to the overlapped defects kinetics.

TABLE IV. Best $N(0)$ fit values obtained before the normalization routine, used to reproduce the kinetics in Figs. 9 and 10, respectively.

$N(0)$ (dB/m)	STH$_1$/GeX	STH$_2$	s-a STH$_1$	s-a STH$_2$	GeY	Cl^0	Ge-STH
PSC (RT)	3					3.3	
PSC (LNT)	1.05	0.29	0.08	0.18			
F (RT)	6					19	
F (LNT)	1.26	0.4	0.18	0.13			
Ge (RT)	14				0.3		
Ge (LNT)	10	8.2	3	0.83	0.6		0.02
Ge + F (RT)	7.6				0.1		
Ge + F (LNT)	9.8	3.4	1.4	1.2	0.3		

TABLE VI. Best fit β parameter used to reproduce the kinetics in Figs. 9 and 10, respectively.

B	STH$_1$/GeX	STH$_2$	s-a STH$_1$	s-a STH$_2$	GeY	Cl^0	Ge-STH
PSC (RT)	0.14					0.27	
PSC (LNT)	0.42	0.34	0.36	0.1			
F (RT)	0.13					0.16	
F (LNT)	0.55	0.32	0.28	0.2			
Ge (RT)	0.15				0.15		
Ge (LNT)	0.49	0.25	0.34	0.25	0.29		0.54
Ge + F (RT)	0.16					0.15	
Ge + F (LNT)	0.55	0.35	0.45	0.15	0.6		

kinetics reflect the irradiation temperature slowing down effect: indeed, the difference is due probably to defects that could be present at RT too but are unstable and bleached in a time scale faster than the current experimental measurement setup. Their contribution to RIA at RT consequently appears negligible.

In a similar way, the defect decay kinetics responsible for the RIA in Ge- and Ge + F-doped fibers at both temperatures were extracted. The obtained results are reported in Fig. 10 with the corresponding fit obtained using the fractal model. At LNT, the Si-STH-related absorption bands have the highest recovery rate, while the Ge-STH seems more stable. The STH-defect instability shows their contribution to be negligible in the RIA spectra of the Ge- and Ge + F-doped optical fibers at RT. To better compare the different kinetic behaviors, the best fitting values are listed in Tables IV–VI, reporting, respectively, the values of N(0), k, and β. It is important to note that the N(0) value in Table IV is the one obtained before applying the normalization routine.

The N(0) values are proportional to the defect concentrations after the x-ray pulse. Coherently with what is expected, the kinetic decay rate, described by the k value, is higher for the faster kinetics. In particular, this parameter can quantify the temperature slowing down effect in the defect kinetics. Indeed, comparing the centers observed at both temperatures, the variety of Si- and Ge-related defects present k values higher than $10^2\,\text{s}^{-1}$ at RT, while at LNT, these values are lower than $1\,\text{s}^{-1}$.

TABLE V. Best fit k parameter used to reproduce the kinetics in Figs. 9 and 10, respectively.

k (S^{-1})	STH$_1$/GeX	STH$_2$	s-a STH$_1$	s-a STH$_2$	GeY	Cl^0	Ge-STH
PSC (RT)	155					0.02	
PSC (LNT)	0.0001	0.001	0.018	1.5			
F (RT)	64					0.24	
F (LNT)	0.0004	0.008	0.065	0.5			
Ge (RT)	1540				2500		
Ge (LNT)	0.014	0.42	0.16	34	0.038		0.007
Ge + F (RT)	1500				2000		
Ge + F (LNT)	0.0024	0.009	0.19	40	0.006		

A very important feature shown by our analysis involves the similarity between the GeX and GeY kinetics in both germanosilicate fibers and at both temperatures, as highlighted by the close values for the parameters given in Tables IV–VI. Even if the temperature strongly affects the recovery rates, the two defects follow the same kinetics. To better highlight this relationship between these two defects, not yet identified, we investigate the GeY absorption band area dependence on the GeX area, as depicted in Fig. 11.

These results show a good linear dependency between the GeY and GeX kinetics for all the tested conditions and fibers. Even if dedicated experiments are needed to determine the nature of this relationship, two hypotheses could be suggested to explain this linear tendency: the first one is that the two defects could be generated from the same precursor site and could also recombine; the second one is that the two absorption bands could indeed be related to the same defect structure.

It could be interesting to compare this behavior with the observations done in Ref. 30 under γ-ray steady state irradiation, in which an anti-correlation has been clearly shown between the intensities of the GeX and GeY absorption bands as a function of the temperature of irradiation. This apparent contradiction could be understood considering different thermal bleaching efficiencies for the two defects generated simultaneously from the same precursor site. The first hypothesis seems then more probable than the second that could not explain the results in Ref. 30. According to this framework, under pulsed ionizing irradiation, the same precursor site generates both GeY and GeX defects, and these defects mostly recover by direct recombination, justifying the linear correlation of the recovery kinetics at fixed temperature. Under steady state irradiation and varying the temperature of irradiation, it is evident[30] that an additional process related to thermal bleaching should be considered. The GeY bleaching is more efficient than the one of GeX (almost flat as a function of the temperature in the tested range), justifying that an anti-correlation between GeX and GeY can be observed as a function of the irradiation temperature.

From our dataset, finally, it appears possible to study in more depth the STHs' impact on the Ge-doped fiber radiation responses at LNT. To this purpose, Fig. 12 compares the kinetics of the normalized STHs' kinetic areas of all the tested canonical samples. Furthermore, since the GeX absorption band overlaps strongly with the STH$_1$ one, assuming the same behavior during the fitting
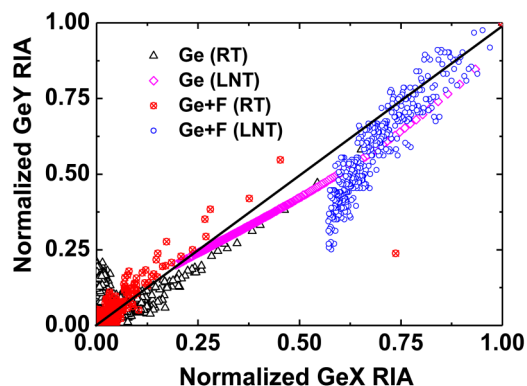
FIG. 11. Dependence of the normalized GeY related RIA vs the normalized GeX related RIA. In black triangles, the GeY RIA measured for the Ge-doped OF at RT and in pink diamonds at LNT, while in red and blue circles are the ones obtained for the Ge + F-doped OF at RT and LNT, respectively. The black continuous line has a slope of 1.

routine. It is interesting to investigate the possible relationship between these two defects, to understand whether the GeX represents a variety of inherent STH_1 structure, in a matrix disturbed by the germanium presence. The GeX decay kinetics are, thus, compared to the ones of the inherent STH_1 in Fig. 12.

Considering the hypothesis that the GeX could represent a variety of inherent STH_1 structure, when surrounded by germanium atoms, Fig. 12 highlights the strong STHs instability in the Ge-doped fiber in all presented cases: in the presence of Ge, the STH defects are bleached faster than in the PSC optical fiber. This could be assigned to the germanium presence in the silica matrix, which distorts the structure making the STH sites in the lattice

more unstable. The same tendency was observed when comparing the inherent STH_1 and GeX, even if further studies, including theoretical calculations, appear necessary to underline this possible correspondence.

V. CONCLUSION

In the present work, we investigated the basic mechanisms governing the responses of PSC, F-, Ge-, and Ge + F-doped optical fibers when exposed to an x-ray pulse (~10 Gy per shot). To better highlight the role of metastable defects in their transient response, we performed RIA measurements at both RT and LNT; using canonical fibers, we can also discuss the fluorine doping influence in the core on fiber radiation sensitivity. The experiments were done online, investigating the RIA in a spectral range between 0.8 eV and 3.2 eV, following the RIA spectra evolution in the ms to 200 s range. To identify the origins of the RIA in the tested ranges, we performed a Gaussian decomposition of the measured RIA spectra using point defect sets already known to be related to the dopants present in the fibers. From this analysis, our work reveals that the fluorine presence in the fiber core seems to reduce the precursor site concentration, such as strained Si–O–Si bonds, leading to a decrease in the RIA caused by the strain-assisted STHs, in agreement with Refs. 33 and 34. For the PSC and F-doped OFs, at both RT and LNT, the defect sets reproduce the measured RIA in the UV/visible range quite well. The observed differences between the RIA spectra at RT and LNT are explained by the stronger contribution of STHs' related absorption bands at LNT. Regarding the NIR range, the RIA origins remain still unresolved in this part of the spectrum, and additional studies are required. However, for the two Ge- and Ge + F-doped fibers, the used defect set is available to reproduce the RIA in the whole investigated spectral range, from the UV to the NIR. The major result of this work is not only to provide a description of the defects responsible to attenuation,
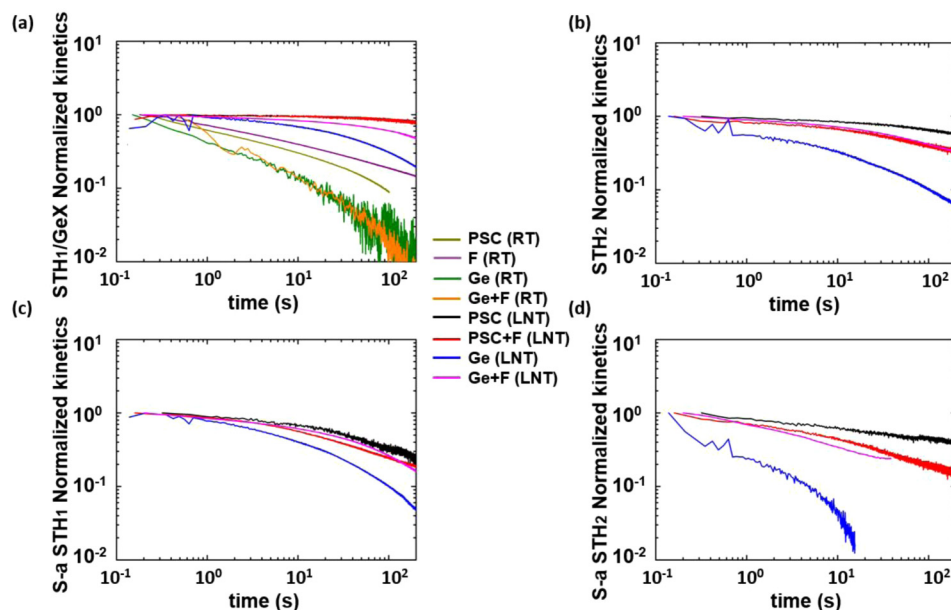

FIG. 12. Normalized STH-related absorption bands area obtained by the fitting routine for all the samples. Inherent STH_1 for the PSC and F-doped and GeX for Ge- and Ge + F-doped fibers (a), inherent STH_2 (b), strain-assisted STH_1 (c), and strain assisted STH_2 (d).

between RT and LNT, of the Ge-doped fiber, but we have also reported a linear correlation between the kinetics of GeY and GeX absorption bands. The nature of this correspondence needs further investigations to be clarified. Moreover, our data highlight a strong STHs contribution in the germanosilicate optical fiber response at LNT in the [1.5 eV−2.7 eV] spectral range. Based on our experimental results, we suggest the GeX center as a Ge-variant of the inherent STH_1. By the way, comparing the LNT decay kinetics of the STHs in PSC and Ge-doped glasses, it seems that the Ge presence is associated with a greater STHs instability. Further experiments are necessary to investigate the physics at stake at shorter times (<1 ms) after the pulse to assess infrared RIA origins in pure silica and F-doped optical fibers. This experimental work might merit additional theoretical investigations, through *ab initio* calculations, of the STH properties in the presence of Ge atoms.

DATA AVAILABILITY

The data that support the findings of this study are available from the corresponding author upon reasonable request.

REFERENCES

[1] K. Kao and G. Hockham, "Dielectrics-fiber surface waveguides for optical frequencies," Proc. IEEE **113**(7), 1151–1158 (1996).

[2] D. A. Krohn, T. W. MacDougall, and A. Mendez, in *Fiber Optics Sensors Fundamentals and Applications*, 4th ed. (SPIE Press, 2015).

[3] A. H. Hartog, in *An Introduction to Distributed Optical Fiber Sensors*, 1st ed. (CRC Press, 2018).

[4] S. Girard, J. Kuhnhenn, A. Gusarov, B. Brichard, M. Van Uffelen, Y. Ouerdane, A. Boukenter, and C. Marcandella, "Radiation effects on silica-based optical fibers: Recent advances and future challenge," IEEE Trans. Nucl. Sci. **60**(3), 2015–2036 (2013).

[5] S. Girard, A. Morana, A. Ladaci, T. Robin, L. Mescia, J.-J. Bonnefois, M. Boutillier, J. Mekki, A. Paveau, and B. Cadier, "Recent advantages in radiation-hardened fiber-based technologies for space applications," J. Opt. **20**(9), 093001 (2018).

[6] J.-L. Bourgade, V. Allouche, J. Baggio, C. Bayer, F. Bonneau, C. Chollet, S. Darbon, L. Disdier, D. Gontier, M. Houry, H.-P. Jacquet, J. P. Jadaud, J.-L. Leray, I. Masclet-Gobin, J.-P. Negre, J. Raimbourg, B. Villette, I. Bertron, J. M. Chevalier, J.-M. Favier, J. Gazave, J.-C. Gomme, F. Malaise, J.-P. Seaux, V. Y. Glebov, I. P. Jaanimag, C. Stoeckl, T. C. Sangster, G. Pien, R. A. Lerche, and E. R. Hodgson, "New constraints for plasma diagnostics development due to the harsh environment of MJ class lasers," Rev. Sci. Instrum. **75**(10), 4204–4212 (2004).

[7] B. Brichard, "Optical fibers based systems for nuclear facilities: From radiation hardening to applications," Thèse de Doctorat (Université de Montpellier, 2008).

[8] S. Girard, Y. Ouerdane, A. Boukenter, C. Marcandella, J. Bisutti, J. Baggio, and J.-P. Meunier, "Integration of optical fibers in megajoule class laser environments: Advantages and limitations," IEEE Trans. Nucl. Sci. **59**(4), 1317–1322 (2012).

[9] LMJ, see http://www-lmj.cea.fr/ for more information about the French facility devoted to fusion by inertial confinement.

[10] NIF, see https://lasers.llnl.gov/ for more information about the US facility devoted to fusion by inertial confinement.

[11] E. J. Friebele, C. G. Askins, M. E. Gingerich, and K. J. Long, "Optical fibers waveguides in radiation environments, II," Nucl. Instrum. Methods Phys. Res. Sect. B **1**(2-3), 355–369 (1984).

[12] S. Girard, Y. Ouerdane, G. Origlio, C. Marcandella, A. Boukenter, N. Richard, J. Baggio, P. Paillet, M. Cannas, J. Bisutti, J.-P. Meunier, and R. Boscaino, "Radiation effects on silica-based preforms and optical fibers—I: Experimental study with canonical samples," IEEE Trans. Nucl. Sci. **55**(6), 3473–3482 (2008).

[13] S. Girard, N. Richard, Y. Ouerdane, G. Origlio, A. Boukenter, L. Martin-Samos, P. Paillet, J.-P. Meunier, J. Baggio, M. Cannas, and R. Boscaino, "Radiation effects on silica-based preforms and optical fibers—II: Experimental study with canonical samples," IEEE Trans. Nucl. Sci. **55**(6), 3508–3514 (2008).

[14] S. Girard, A. Alessi, N. Richard, L. Martin-Samos, V. De Michele, L. Giacomazzi, S. Agnello, D. Di Francesca, A. Morana, B. Winkler, I. Reghioua, P. Paillet, M. Cannas, T. Robin, A. Boukenter, and Y. Ouerdane, "Overview of radiation induced point defects in silica-based optical fibers," Rev. Phys. **4**, 100032 (2019).

[15] V. De Michele, A. Morana, C. Campanella, J. Vidalot, A. Alessi, A. Boukenter, M. Cannas, P. Paillet, Y. Ouerdane, and S. Girard, "Steady state x-ray radiation induced attenuation in canonical optical fibers," IEEE Trans. Nucl. Sci. **67**, 1650–1657 (2020).

[16] S. Girard, V. De Michele, A. Alessi, C. Marcandella, D. Di Francesca, P. Paillet, A. Morana, J. Vidalot, C. Campanella, S. Agnello, M. Cannas, M. Gaillardin, E. Marin, A. Boukenter, and Y. Ouerdane, "Transient and steady-state radiation response of phosphosilicate optical fibers: Influence of H2 loading," IEEE Trans. Nucl. Sci. **67**(1), 289–295 (2020).

[17] D. Di Francesca, S. Girard, S. Agnello, C. Marcandella, P. Paillet, Y. Ouerdane, Y. Kadi, M. Brugger, and A. Boukenter, "Combined temperature radiation effects and influence of drawing conditions on phosphorus-doped optical fibers," Phys. Status Solidi A **216**, 1800553 (2019).

[18] S. Girard, D. L. Griscom, J. Baggio, B. Brichard, and F. Berghmans, "Transient optical absorption in pulsed-X-ray-irradiated pure-silica-core optical fibers: Influence of self-trapped holes," J. Non-Cryst. Solids **352**, 2637–2642 (2006).

[19] S. Girard and C. Marcandella, "Transient and steady state radiation responses of solarization-resistant optical fibers," IEEE Trans. Nucl. Sci. **57**(4), 2049–2055 (2010).

[20] P. F. Kashaykin, A. L. Tomashuk, M. Yu. Salgansky, A. N. Guryanov, and E. M. Dianov, "Anomalies and peculiarities of radiation-induced light absorption in pure silica optical fibers at different temperatures," J. Appl. Phys. **121**, 213104 (2017).

[21] V. De Michele, C. Marcandella, D. Di Francesca, P. Paillet, A. Alessi, M. Cannas, Y. Ouerdane, A. Boukenter, and S. Girard, "Pulsed x-ray radiation responses of solarization-resistant optical fibers," Phys. Status Solidi A **216**, 1800487 (2018).

[22] D. L. Griscom, "Self-trapped holes in amorphous silicon dioxide," Phys. Rev. B **40**(6), 4224–4227 (1989).

[23] D. L. Griscom, "Electron spin resonance characterization of self-trapped holes in amorphous silicon dioxide," J. Non-Cryst. Solids **149**(1-2), 137–160 (1992).

[24] E. M. Dianov, V. N. Karpechev, V. O. Sokolov, V. B. Sulimov, P. V. Chernov, L. S. Kornienko, I. O. Morozova, and A. O. Rybaltovskiin, "Spectroscopic manifestations of self-trapped holes in silica theory and experiment," Phys. Status Solidi B **156**(2), 663–675 (1989).

[25] L. Skuja, K. Kajihara, K. Smits, A. Silins, and H. Hosono, "Luminescence and Raman detection of molecular Cl_2 and ClClO molecules in amorphous SiO_2 matrix," J. Phys. Chem. C **121**(9), 5261–5266 (2017).

[26] D. L. Griscom, E. J. Friebele, and S. P. Mukherjee, "Studies of radiation-induced point defects in silica aerogel monoliths," Cryst. Lattice Defects Amorphous Mater. **17**, 157–163 (1987).

[27] E. J. Friebele, D. L. Griscom, and G. H. Sigel, "Defect centers in a germanium-doped silica-core optical fiber," J. Appl. Phys. **45**(8), 3424–3428 (1974).

[28] V. B. Neustruev, "Colour centres in germanosilicate glass and optical fibres," J. Phys. Condens. Matter **6**(35), 6901–6936 (1994).

[29] G. Origlio, "Properties and radiation response of optical fibers: Role of dopants," Ph.D. thesis (Unversité Jean Monnet St Etienne, 2010).

[30] P. F. Kashaykin, A. L. Tomashuk, V. F. Khopin, A. N. Guryanov, S. L. Semjonov, and E. M. Dianov, "New radiation colour center in germanosilicate glass fibres," Quantum Electron. **48**(12), 1143–1146 (2018).

[31]P. F. Kashaykin, A. L. Tomashuk, V. F. Khopin, S. V. Firstov, A. N. Guryanov, and E. M. Dianov, "Observation of radiation-induced absorption of self-trapped holes in Ge-doped silica fibers in near infrared range at reduced temperature," J. Non-Cryst. Solids **496**, 24–28 (2018).

[32]H. Hosono, M. Mizuguchi, L. Skuja, and T. Ogawa, "Fluorine-doped SiO_2 glasses for F_2 excimer laser optics: Fluorine content and color-center formation," Opt. Lett. **24**(22), 1549–1551 (1999).

[33]S. Girard, C. Marcandella, G. Origlio, Y. Ouerdane, A. Boukenter, and J.-P. Meunier, "Radiation-induced defects in fluorine-doped silica-based optical fibers: Influence of a pre-loading with H_2," J. Non-Cryst. Solids **355**, 1089–1091 (2009).

[34]S. Girard, C. Marcandella, A. Alessi, A. Boukenter, Y. Ouerdane, N. Richard, P. Paillet, M. Gaillardin, and M. Raine, "Transient radiation responses of optical fibers: Influence of MCVD process parameters," IEEE Trans. Nucl. Sci. **59**(6), 2894–2901 (2012).

[35]A. Johan, B. Azaïs, C. Malaval, G. Raboisson, and M. Roche, "ASTERIX: a new facility for simulation of dose rate effects on electronics," Ann. Phys. **14**(6), 379–393 (1989).

[36]S. Girard, J. Baggio, J.-L. Leray, J.-P. Meunier, A. Boukenter, and Y. Ouerdane, "Vulnerability of optical fibers for laser mégajoule facility: Preliminary studies," IEEE Trans. Nucl. Sci. **52**, 1497–1503 (2005).

[37]S. Girard, Y. Ouerdane, B. Vincent, J. Baggio, K. Medjahdi, J. Bisutti, B. Brichard, A. Boukenter, A. Boudrioua, and J.-P. Meunier, "Spectroscopic study of γ-ray and pulsed x-ray radiation-induced point defects in pure-silica-core optical fibers," IEEE Trans. Nucl. Sci. **54**(4), 1136–1142 (2007).

[38]See https://ixblue.com for detailed information of the company which manufactured the FUT OFs.

[39]L. Skuja, "Optical properties of defects in silica," in *Defects in and Related Dielectrics Science and Technology (NATO Science Series II)*, edited by G. Pacchioni, L. Skuja, and D. L. Griscom (Kluwer, Dordrecht, 2000), pp. 73–116.

[40]M. Cannas, L. Vaccaro, and B. Boizot, "Spectroscopic parameters related to non-bridging oxygen hole centers in amorphous-SiO_2," J. Non-Cryst. Solids **352**(3), 203–208 (2006).

[41]A. Alessi, S. Girard, M. Cannas, S. Agnello, A. Boukenter, and Y. Ouerdane, "Influence of drawing conditions on the properties and radiation sensitivities of pure-silica-core optical fibers," J. Lightwave Technol. **30**(11), 1726–1732 (2012).

[42]K. Nagasawa, M. Tanabe, and K. Yahagi, "Gamma-ray-induced absorption bands in pire-silica-core fibers," Jpn. J. Appl. Phys. **23**(12), 1608–1613 (1984).

[43]D. L. Griscom, "Trapped-electron centers in pure and doped glassy silica: A review and synthesis," J. Non-Cryst. Solids **357**(8-9), 1945–1962 (2011).

[44]P. F. Kashaykin, A. L. Tomashuk, I. S. Azanova, O. L. Vokhmyanina, T. V. Dimakova, I. A. Maltsev, Y. O. Sharonova, E. A. Pospelova, O. M. Tatsenko, A. V. Filippov, N. S. Kuzyakina, O. V. Zverev, and E. M. Dianov, "Radiation induced attenuation in pure silica polarization maintaining fibers," J. Non-Cryst. Solids **508**, 26–32 (2019).

[45]S. Girard, J. Baggio, and J. Bisutti, "14-MeV neutron, γ-ray, and pulsed x-ray radiation-induced effects on multimode silica-based optical fibers," IEEE Trans. Nucl. Sci. **53**(6), 3750–3757 (2006).

[46]S. Girard, C. Marcandella, A. Morana, J. Perisse, D. Di Francesca, P. Paillet, J.-R. Macé, A. Boukenter, M. Léon, M. Gaillardin, N. Richard, M. Raine, S. Agnello, M. Cannas, and Y. Ouerdane, "Combined high dose and temperature radiation effects on multimode silica-based optical fibers," IEEE Trans. Nucl. Sci. **60**(6), 4305–4313 (2013).

[47]D. L. Griscom, "Fractal kinetics of radiation-induced point-defect formation and decay in amorphous insulators: Application to color centers in silica-based optical fibers," Phys. Rev. B **64**, 174201 (2001).